

Concurrent Polyvalent Interaction and Electrocatalysis to Improve Lithium-Sulfur Battery Performance

Subramani Kumar (சுப்பிரமணி குமார்)^[a, b] and Kothandam Krishnamoorthy (கோதண்டம் கிருஷ்ணமூர்த்தி)*^[a, b]

Dedicated to Dr. S. Sivaram on the occasion of his 75th birthday.

Batteries with improved efficiency are desired. Li–S batteries are attractive due to their high specific capacity and energy density. However, sluggish sulfur redox reaction and polysulfide dissolution are significant challenges in Li–S batteries. In this work, we report graphene with doped layer to electrocatalyze the sluggish sulfur redox reaction. The doped layer comprises heteroatoms such as either N or N and S. The doped layer also comprises cations of Ni. We have chosen a “doped layer on graphene” over “doped graphene” to avoid defects in the basal plane of graphene. We found the doped layer comprising

graphene (DLC–G) to electrocatalyze the polysulfide redox reaction. However, the interaction between the doped layer and polysulfide is still weak, hence the dissolution is not suppressed. To circumvent the polysulfide dissolution, graphene with cationic layer was prepared. We found that cations in the layer electrostatically attract the polysulfides due to the polyvalent interaction. Thus, the dissolution is suppressed. While using this material in the Li–S batteries, the specific capacity, energy density and power density were found to be 1345 mAh g⁻¹, 782 Wh kg⁻¹ and 4437 W kg⁻¹, respectively.

1. Introduction

Battery systems with significantly improved energy and power density over the existing lithium-ion batteries are of great interest. Li–S batteries with a theoretical specific capacity of 1675 mAh g⁻¹ and energy density up to 2600 Wh kg⁻¹ are attractive energy storage devices.^[1,2] Despite the promise, Li–S batteries are plagued with issues such as poor electrical conductivity of sulfur (5×10^{-30} S cm⁻¹), sluggish sulfur redox reaction and dissolution of polysulfide in the battery electrolyte.^[3] The poor electrical conductivity issue is tackled by preparing carbon composite electrodes.^[4] The sluggish redox reaction and dissolution of polysulfide remain as challenges.^[5] The two major approaches to circumvent the dissolution of polysulfide, which is commonly known as the shuttle effect can be classified into, i) membrane modification and ii) electrode modification. First, the separator membranes are modified with carbon allotropes, polymers and nanostructures. The modified membranes repel the polysulfides and suppress the deleterious shuttle effect.^[6,7] In the second approach, porous structures of organic and inorganic materials have been used to confine the sulfur. The pores that are used to load the sulfur also render

the possibility of diffusion of polysulfides from the confining material.^[8] Thus, the confinement approach has its limitations. Li–S battery metrics of various materials are summarized in Table S1 (Supporting Information).

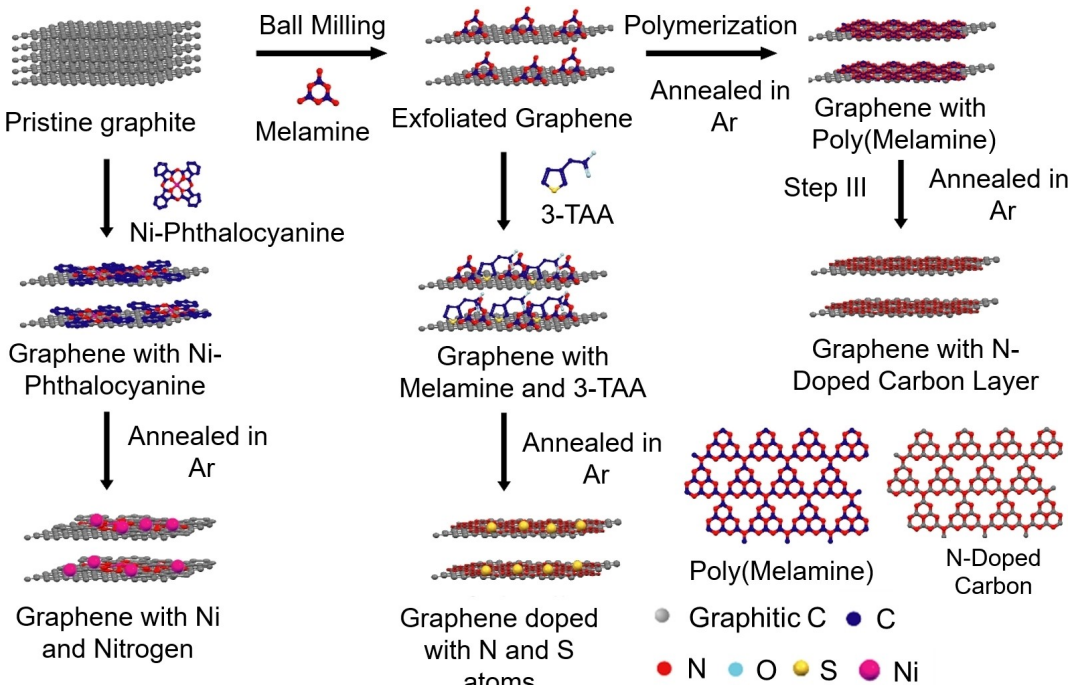
Usually, the battery electrode is prepared by blending sulfur, polymer binder and conducting carbon.^[6] Neither the conducting carbon nor the binder is effective in suppressing the polysulfide dissolution.^[9] Thus, an additive is required. The additive should be a material with properties to withhold the polysulfide from dissolving in the electrolyte. With its excellent properties and easy synthesis, graphene seems to be an attractive candidate.^[10] However, the surface of graphene is hydrophobic; hence it is not suitable to withhold polysulfide.^[11] Therefore, modification of graphene is required. Doped graphene is an option.^[12] It has been used as an additive in the Li–S battery electrodes. All the doped graphene do not have the desired effect. For example, pyridinic and graphitic nitrogen comprising graphenes are better electrocatalysts than pyrrolic nitrogen-containing graphene.^[13] The pyridinic and pyrrolic nitrogens are Lewis base and they can attract Lewis acid such as polysulfides. However, it has been shown that the pyridinic nitrogens are present either on the edges or at the defect sites of graphene, which is a limitation. Thus, an approach that renders the possibility of preparing graphene without defect but with pyridinic and graphitic nitrogen is required. To accomplish this paradoxical objective, we resorted to an approach that mechanically peels off graphene from graphite in presence of exfoliator. The exfoliator molecules that adhere to the graphene surface have been judiciously chosen to have desired dopant atoms. The graphene preparation approach is mechanical; hence the graphene’s basal plane is unaffected.^[14–16] In the first set of experiments, melamine (Scheme 1) was used as exfoliator. Graphite and melamine are

[a] S. Kumar (சுப்பிரமணி குமார்), Dr. K. Krishnamoorthy (கோதண்டம் கிருஷ்ணமூர்த்தி)

Polymer Science and Engineering Division
CSIR-National Chemical Laboratory
Pashan Road, Pune 411008, India

[b] S. Kumar (சுப்பிரமணி குமார்), Dr. K. Krishnamoorthy (கோதண்டம் கிருஷ்ணமூர்த்தி)
Academy of Scientific and Innovative Research
Kamla Nehru Nagar, Ghaziabad 201002, India
E-mail: k.krishnamoorthy@ncl.res.in

 Supporting information for this article is available on the WWW under
<https://doi.org/10.1002/batt.202100229>



Scheme 1. Cartoon showing the steps involved in the preparation of DLC-G.

ball-milled in planetary ball milling equipment. After exfoliation, the samples were subjected to thermal treatment. During this process, melamine undergoes thermal polymerization leading to a cross-linked polymer that can act as a source of nitrogen-doped carbon.^[17] Upon further heating, we envisioned graphenes with a layer comprising pyridinic and graphitic nitrogen (Scheme 1). We reiterate that a minimal amount of defects are anticipated in the basal plan of graphene because the exfoliation is mechanical. Dual doping can enhance electrocatalysis,^[18] hence we prepared graphene with layers comprising S and N atoms. These modified graphene samples are expected to electrocatalyze the sluggish polysulfide redox reaction.^[19] We understand that the N and S comprising graphene layer alter the surface properties, but the interaction between polysulfide and graphene is weak. The sulfur undergoes various structural changes; hence covalent immobilization is not an option. Therefore, we need to rely on non-covalent, yet strong interaction. The negative charges on polysulfide render the possibility to anchor them on the surface of graphene non-covalently. In order to achieve this objective, we must prepare graphene layer with positive charges. Our approach, mechanical exfoliation, renders the possibility of embedding cations on the layer of graphene. To embed cations on the layer of graphene, graphite was ball milled with Nickel Phthalocyanine (Scheme 1). During the milling process, Nickel Phthalocyanine molecules adhere to the surface of graphene. Subsequent heating of the sample resulted in the formation of graphene with a carbon layer comprising nickel ions and nitrogen. The nitrogen-doped carbon layer is expected to catalyze the sulfur redox reaction,^[20] concurrently the nickel ions are expected to suppress polysulfide dissolution due to electrostatic polyvalent interaction.^[21] Various interactions have

been used to suppress polysulfide dissolution in Li–S batteries. Electrostatic polyvalent interaction, which is a very strong interaction hasn't been used in Li–S batteries. Probably due to the difficulty in using cations that can have polyvalent electrostatic attractions with polysulfide. Herein, we report a method to immobilize cations on graphene that interact with polysulfide due to polyvalent electrostatic attraction. Indeed, the Ni cation and N containing carbon layer based graphene exhibits superior battery performance that is reported in this research work.

2. Results and Discussion

Graphite was ball milled with melamine (exfoliator) at various revolutions per minute (RPM). We also varied the duration of the ball milling. In another set of experiments, anthracene (control molecule, Scheme 1) was used as an exfoliator (Table S2, Supporting Information). Anthracene has been chosen as a control molecule due to the absence of heteroatoms. After the ball milling, the samples were washed with a copious amount of DMF to remove excess exfoliators. The results and discussions are divided into four sections. First, we discuss the characterization of graphene with an exfoliator. In the next section, the preparation and characterization of DLC-G are discussed. Subsequently, battery fabrication and testing are discussed. In the fourth section, we will discuss the preparation and characterization of DLC-G with Ni ions and battery performance using the same material. After ball milling and washing, the samples were subjected to Raman spectroscopic analysis. Intense G and 2D bands appeared at 1581 and 2676 cm⁻¹, respectively (Figure 1a). D band appeared at

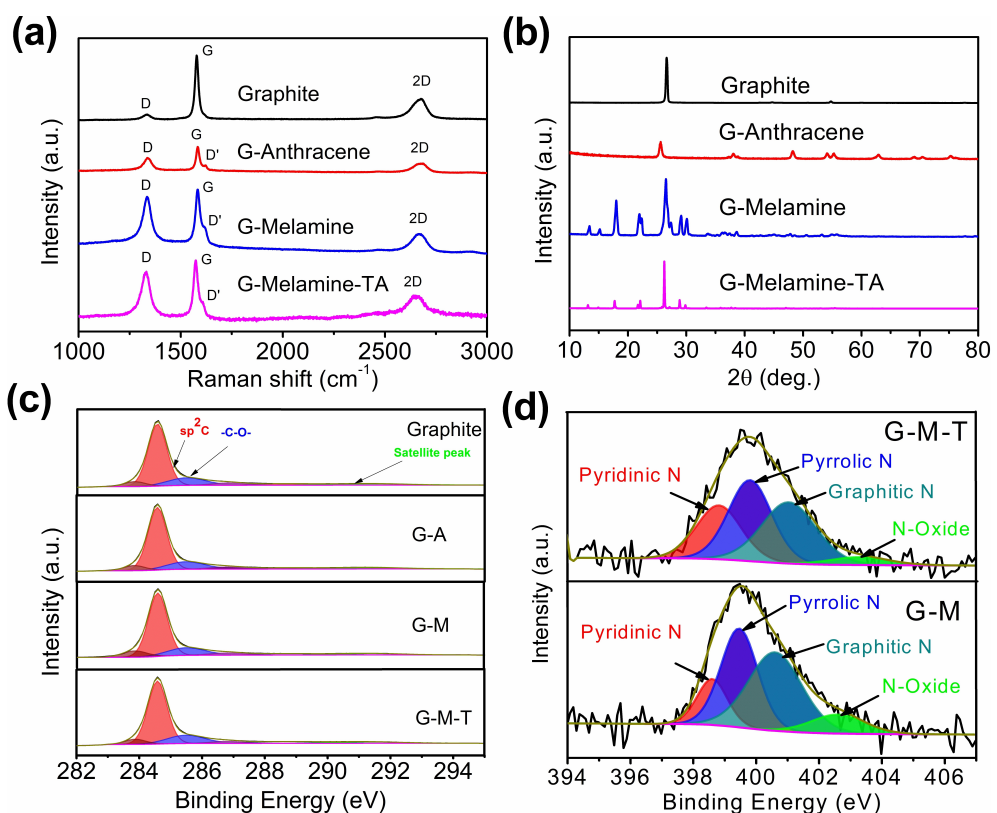


Figure 1. Raman spectra showing D, D', G and 2D bands of exfoliated graphene (a) and XRD pattern of exfoliated graphene (b). XPS spectra of pristine graphite, few-layer graphene G-A, G-M and G-M-T (c) and deconvoluted peaks of the nitrogen region for G-M and G-M-T (d).

1335 cm⁻¹ and D' shoulder appeared at 1616 cm⁻¹. The intensity of D and G bands (I_D/I_G) ratio provides information about the graphene layers.^[14,22] High I_D/I_G value is an indication of fewer layer graphenes. The highest I_D/I_G of 0.90 was found while melamine was used as exfoliator with RPM of 200. The duration of the milling was 60 min. All the parameters used for milling and the properties of resultant materials are listed in Table S2. The I_D/I_D' provides information about defects in the graphene. I_D/I_D' of 3.5 or lower indicates edge and boundary defects with no SP³ defects.^[23] All the samples showed I_D/I_D' less than 3.5 indicating the formation of high-quality graphene while using melamine and anthracene as exfoliators (Table S2). The samples were subjected to XRD analysis, which is an effective method to identify the formation of graphene from graphite through the mechanical exfoliation process. Graphene shows an intense peak at 2θ of 26.6° that corresponds to 002 plane (Figure 1b).^[15] The d-spacing for graphite was found to be 3.347 Å, which increased to 3.377 Å while using melamine as an exfoliator. This was further increased to 3.384 Å while using anthracene as an exfoliator. Thus, the exfoliators increase the distance between the layers of graphene. With this information in hand, we proceeded to synthesize DLC-G. The exfoliated graphene was heated at 600 °C in an inert atmosphere. Henceforth, the graphene prepared with anthracene as an exfoliator will be mentioned as G-A. The graphene prepared using melamine as an exfoliator will be mentioned as G-M. The G-M comprises nitrogen atoms in the layer. To prepare N and S

comprising DLC-G, the melamine exfoliated graphene was treated with 3-thiophene acetic acid (TAA) (Scheme 1). The carboxylic acid functionality of TAA interacts with pyridinic and amine moieties of melamine. Thermal treatment of this sample is envisioned to yield N and S comprising DLC-G. This sample will be mentioned as G-M-T in all the forthcoming discussions.

After heating, the samples were subjected to XPS analysis. The XPS spectra of graphite showed the presence of sp² C (284.6 eV) (Figure 1c). We also found a peak corresponding to -C-O- (285.6 eV) (Figure 1c). The small peak at 283.8 eV is due to disordered carbon.^[24] The G-A also showed these peaks indicating the absence of any new heteroatoms due to the lack of them in anthracene. The XPS spectra of G-M showed N1s peak at 399 eV and other characteristic peaks found for G-A. The G-M-T showed a peak at 165 eV that is characteristic of -C=S-C- moieties (Supporting Information, Figure S1). These experiments have proven that the DLC-G with various dopants can be synthesized by changing the exfoliator molecules. As mentioned in the introduction section, three types of nitrogens are present in doped graphenes. We anticipate those in the DLC-G. In the case of G-M, the pyridinic nitrogen is lowest at 24.8%, and the pyrrolic nitrogen is highest at 36.1% (Figure 1d). In the case of G-M-T, the graphitic nitrogen is highest at 40.9%, and the pyridinic nitrogen is 13.5%. The high graphitic nitrogen in G-M-T may lead to better electrocatalytic activity. Atomic mapping was carried out to corroborate the presence of heteroatoms in the samples. The G-A samples

showed the presence of carbon throughout the sample (Supporting Information, Figure S2). In the case of G–M, carbon and nitrogen were also present and they are distributed uniformly throughout the sample (Supporting Information, Figure S3). We noticed the presence of sulfur in the samples of G–M–T (Supporting Information, Figure S4). The TEM images showed a clear difference in morphology between the graphite and graphene. The graphite comprises about 80 layers of graphene (Supporting Information, Figure S5). About ten and five layers are found in G–M (Figure 2a) and G–M–T (Figure 2b), respectively. TEM imaging was carried out for samples blended with sulfur. The sulfur loading did make the graphene opaque (Figure 2c). The opaqueness is due to the presence of a large amount of sulfur along with DLC–G. We hypothesized that the DLC–G would withhold sulfur better than that of graphite. To test this hypothesis, the samples were subjected to TGA analysis. The sulfur loading was 85.8% while sulfur was blended with G–A. It increased to 87.2% and 89.5% for G–M and G–M–T, respectively (Figure 2d). Thus, the doped layer on the DLC–G increased the sulfur loading. We also carried out polysulfide adsorption experiment to find out the interaction between DLC–G and polysulfides. A 5 mM Li_2S_6 was prepared by following the reported procedure.^[25] In that solution, an internal standard diketopyrrolopyrrole (DPP) was added. From the stock solution, 5 mL was distributed into various glass vials. To that solution, 5 mg of DLC–G was added and the solution was left quiescent for 12 hrs. The color of the solution with G–A didn't vary significantly, indicating the weak interaction between polysulfide and G–A. To quantify the interaction, an aliquot was taken to record UV-vis absorption spectra. The Li_2S_6 solution

showed three peaks at 263, 281 and 338 nm. The solution with DPP (internal standard) showed two additional peaks at 510 and 547 nm. The UV-vis absorption spectra of the aliquot solution are shown in Figure 2e. The absorption maxima decreased in the following order G–A > G–M > G–M–T. This trend indicates that the G–A has weak and G–M–T has strong interaction with polysulfides. In case of G–A, there is no specific interaction between the hydrophobic surface of G–A and negative charge bearing polysulfides. On the other hand, polysulfide interacts with G–M due to Lewis acid base interaction. In case of G–M–T, Lewis acid base interaction and sulfur–sulfur interaction is in operation. Due to the strong interaction, polysulfide adhered well on to the surface of G–M–T. This experiment corroborates our hypothesis that the layer with heteroatom increases the interaction between polysulfide and graphene. With this information in hand, we proceeded to fabricate Li–S batteries. The cells were used to record cyclic voltammetry between 3 and 1.5 V vs. Li^+/Li . The first peak appeared at 2.3 V, which corresponds to the conversion of S_8 to Li_2S_n ($4 < n \leq 8$).^[1] Subsequently, conversion of Li_2S_n to $\text{Li}_2\text{S}_2/\text{Li}_2\text{S}$ occurred at 2 V. In the reverse sweep, conversion of Li_2S to S_8 occurred at 2.4 V (Figure 3a).^[26] These are typical peaks observed in Li–S batteries. It is worth noting the variation in peak current intensity (i_p) as a function of cycle number. At the end of the 5th cycle, the i_p decreased by 25% while using G–A. The corresponding change was 10% while using G–M as electrode. Based on this trend, we anticipated a lower change while using G–M–T as electrode. Contrary to this expectation, the decrease was 29%, which is the highest among the DLC–G. This indicates that the polysulfide dissolution has increased

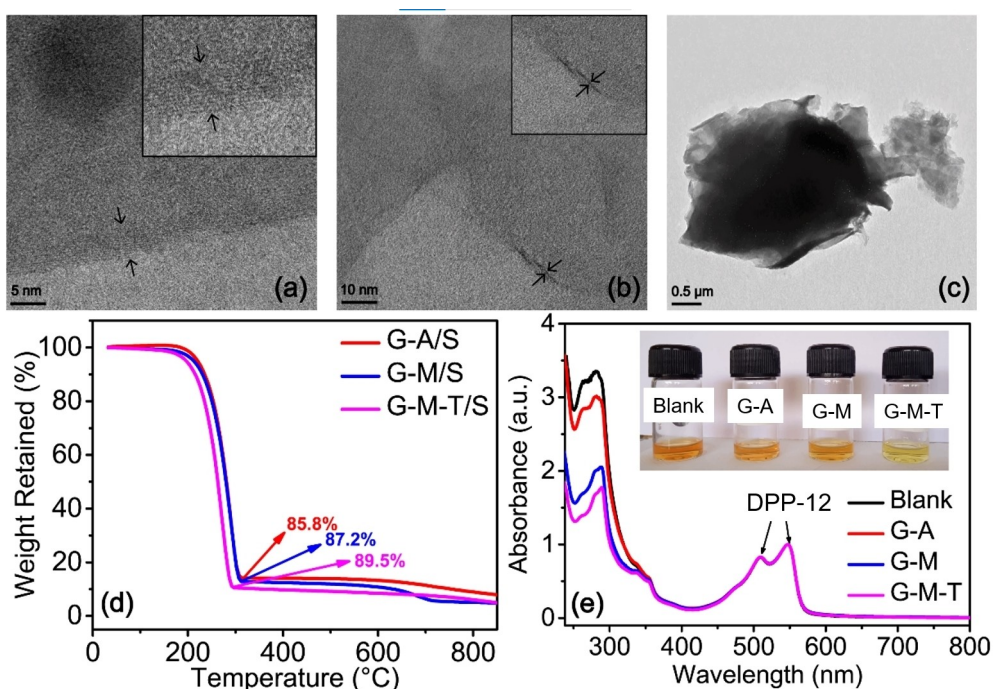


Figure 2. TEM images showing the few layers of graphene G–M (a) and G–M–T (b). TEM image of sulfur loaded G–M–T (c). TGA indicating the sulfur loading in G–A, G–M and G–M–T (d). UV-Vis spectra of Li_2S_6 solution in presence and absence of DLC–G (e). The insert is the photograph of Li_2S_6 solution in presence of DLC–Gs.

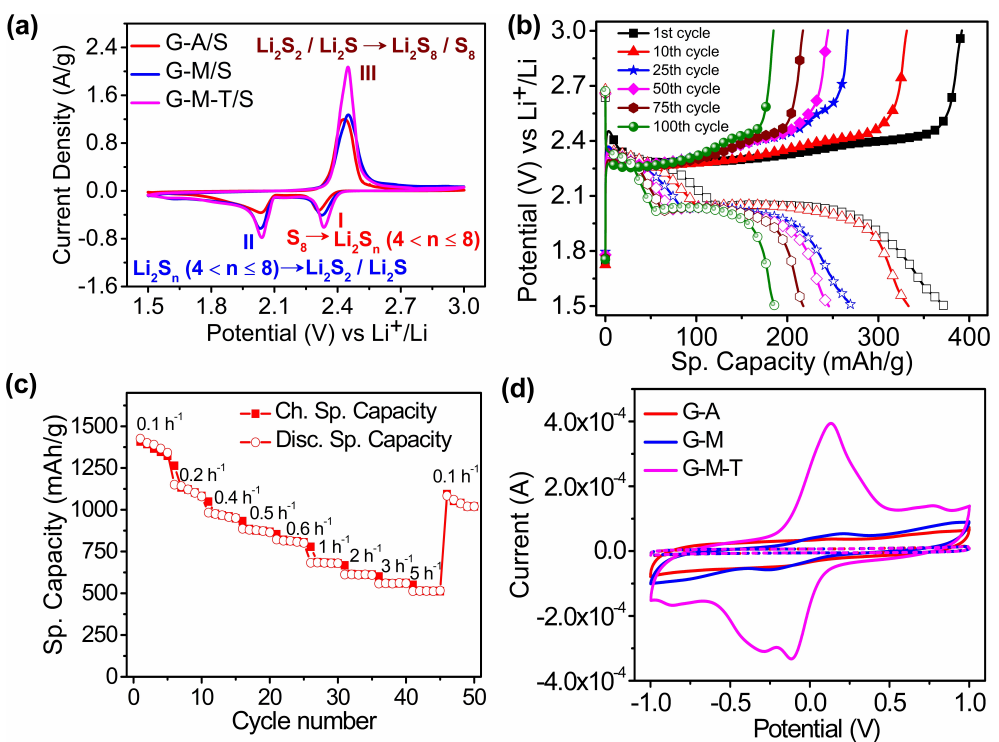


Figure 3. Cyclic voltammogram of Li–S battery comprising various DLC-Gat a scan rate of 0.1 mVs^{-1} (a). Charge-discharge curves at 0.2 h^{-1} , showing specific capacity fading while using G–A in Li–S battery electrode (b). Rate performance study of G–M–T based Li–S battery (c). Plot showing the cyclic voltammograms of symmetric cells with various DLC–G(d)

while the electrodes are prepared with G–M–T. Although the absorption studies (Figure 2e) indicate strong interaction between G–M–T and polysulfides in quiescent solution, the polysulfide dissolution is not suppressed during potential sweep. The i_p was found to be $1.08 \times 10^{-3}\text{ mA}$ for G–A, which increased to $1.15 \times 10^{-3}\text{ mA}$ for G–M and increased further to $1.87 \times 10^{-3}\text{ mA}$ for G–M–T. The significant increase in i_p of sulfur redox in G–M–T based electrodes is an indication of electrocatalysis. The batteries fabricated using DLC–G were subjected to charge-discharge experiments. The experiments were carried out between 1.5 and 3 V vs. Li⁺/Li. The discharge curve showed two plateaus corresponding to the following reactions, $S_8 \rightarrow Li_2S_n$ ($4 < n \leq 8$), Li_2S_n ($4 < n \leq 8$) $\rightarrow Li_2S_2 / Li_2S$ at 2.3 and 2.0 V, respectively.^[1] The reactions corresponding to various regions of the curve are shown in Figure 3a. The specific capacity of the first cycle of the battery with G–A was 372 mAh g^{-1} (0.2 h^{-1}) (Figure 3b). Please note that the specific capacity is a mere 22% of theoretical capacity (1675 mAh g^{-1}). This decreased to 186 mAh g^{-1} at 100th cycle, decreasing 54% compared to the first cycle. A similar decrease in specific capacity as a function of hundred charge-discharge cycles was observed for other C rates. The reduction in specific capacity compared to the first charge-discharge cycle was 35% (1 h^{-1}), 14% (2 h^{-1}) and 44% (5 h^{-1}). These experiments indicate the poor efficacy of DLC–G that is devoid of heteroatoms in Li–S batteries. Furthermore, the polarization of the discharge curve means poor electrocatalysis while using G–A as electrode material. In the case of G–M, the specific capacity of the first cycle was 535 mAh g^{-1} (0.2 h^{-1}), which is 163 mAh g^{-1} higher than that of G–A based

batteries (Supporting Information, Figure S6). We attribute the marginal performance increase to the presence of 24.8% of pyridinic nitrogen in G–M. The decrease in specific capacity as a function of hundred charge-discharge cycling was found to be 42% (311 mAh g^{-1} at 100th cycle). Thus, the performance of G–M (N doped layer comprising graphene) is better than G–A based batteries. The improved performance is attributed to heteroatoms that are present in G–M. At higher C rates, the decrease in specific capacity as a function of hundred charge-discharge cycling was found to be 25% (1 h^{-1}), 14% (2 h^{-1}) and 31% (5 h^{-1}). So far, a battery is subjected to charge-discharge cycling at a particular C rate for hundred cycles. To test a battery's efficacy as a function of various Crates, rate performance studies were conducted. In this experiment, a battery was subjected to charge-discharge cycling at 0.1 h^{-1} and the C rate was gradually increased up to 5 h^{-1} . While increasing the C rate, the specific capacity decreases. At 5 h^{-1} , the specific capacity decreased by 82% compared to 0.1 h^{-1} . This result raises the question, is the massive decrease due to sulfur dissolution? To test this, the battery that was discharged at 5 h^{-1} , was subjected to charge-discharge experiment at 0.1 h^{-1} . In this experiment, the specific capacity bounced back to 634 mAh g^{-1} , which is very close to the specific capacity observed at the start of the experiment (Supporting Information, Figure S7). Please recall the specific capacity at 5 h^{-1} was 124 mAh g^{-1} , which was observed in the previous experiment. Thus, the bounce-back of specific capacity at 0.1 h^{-1} indicates that the polysulfide dissolution is low during charge-discharge experiments, while using G–M.

In the next set of experiments, G–M-T was used to prepare the battery electrodes. The specific capacity of batteries prepared using G–M-T was 1270 mAh g^{-1} , while charge-discharge experiment was carried out at 0.2 h^{-1} (Supporting Information, Figure S8). This value is 898 mAh g^{-1} higher than the control experiment (G–A based batteries). The impressive performance enhancement is attributed to the presence of 40.9% pyridinic nitrogen. The decrease in specific capacity as a function of hundred charge-discharge cycling was found to be 39%. This data indicate the improvement in battery performance imparted by doping the carbon layer with N and S. The rate performance study was conducted by following the procedure adapted for G–M based batteries. At 0.1 h^{-1} , the specific capacity was found to be 1426 mAh g^{-1} . Upon increase in C rate, the specific capacity decreased. The lowest specific capacity of 513 mAh g^{-1} was found at 5 h^{-1} . The decrease is 64%. After the charge-discharge experiments at 5 h^{-1} , the batteries were cycled at 0.1 h^{-1} . The specific capacity was found to be 108 mAh g^{-1} (Figure 3c). This is 75% of the specific capacity observed at the same C rate (0.1 h^{-1}) during the start of the experiment. Thus, the battery didn't recover fully probably due to polysulfide dissolution. Thus, the polysulfide dissolution is higher in case of G–M-T based batteries compared to G–M based batteries. This correlates well with the observation of decrease in peak intensity in cyclic voltammograms of G–M-T based batteries (Figure 3a). To study the electrocatalytic properties of DLC-Gbased batteries, symmetric cells were fabricated. The working and counter electrodes comprise DLC–G, conducting carbon and binder. The electrolyte comprises Li_2S_6 .The cyclic voltammograms (CV) were recorded between -1 and $+1 \text{ V}$ at a scan rate of 5 mVs^{-1} . The CV of G–A showed extremely weak oxidation (0.11 V) and reduction (-0.11 V) wave. G–M also showed oxidation and reduction waves at 0.24 and -0.24 V , respectively (Figure 3d). This indicate poor electrocatalysis by these two DLC–G. Indeed, the CV of symmetric cells without Li_2S_6 in the electrolyte didn't show oxidation and reduction waves (Figure 3d). Thus, the oxidation and reduction waves in the CV of G–A and G–M based symmetric cells originate from Li_2S_6 . The CV of G–M-T showed a sharp oxidation peak at 0.12 V . This peak corresponds to the conversion of lithium sulfide to lithium polysulfide and sulfur. Two peaks were observed during the reverse scan at -0.12 and -0.29 V . The peak at -0.12 V corresponds to the conversion of Li_2S_6 to short chain lithium polysulfide. The peak at -0.29 V corresponds to the formation of lithium sulfide.^[27]

To test the hypothesis that DLC-Gwith Nickel ion and N as an efficient electrocatalyst, graphene was prepared by ball milling graphite with Nickel phthalocyanine. The sample was subsequently heated to get DLC-Gwith Ni ion and N. This sample will be mentioned as G-NP in the forthcoming discussions. The XPS spectra of the sample confirmed the presence of pyridinic nitrogen (38.9%), pyrrolic nitrogen (28.6) and graphitic nitrogen (32.4%) (Supporting Information, Figure S9). The TEM image showed about five layers of graphene in the samples of G-NP (Figure 4a). The elemental mapping showed Ni ion and N are uniformly distributed throughout the sample (Supporting Information, Figure S10). The G-NP was

blended with sulfur and the sample was subjected to TGA analysis. The sulfur content was found to be 89.4%, which is the highest among DLC–G(Figure 4b). To test whether the G-NP has attractive interaction with polysulfides, 5 mg of G-NP was dropped into the 5 mM solution of Li_2S_6 . The solution was left quiescent for 12 hrs. The solution appeared colorless to the naked eyes indicating that the polysulfide is adhered to the positive charge bearing G-NP. An aliquot was taken to record UV-vis absorption spectra. The absorption peaks corresponding to S_6^{2-} showed the lowest absorption among all the DLC–G–(Figure 4c). This corroborates our hypothesis of polyvalent interaction between the Ni cations of G-NP with that of polysulfides. In order to study the electrocatalysis of DLC–G, symmetric cells were fabricated. In these cells, the working and counter electrodes are prepared with same material. The cyclic voltammograms were recorded at a scan rate of 5 mVs^{-1} . In case G-NP based symmetric cells, two well defined oxidation and reduction peaks were observed (Figure 4d). The first oxidation peak centered at 0.09 V , indicates the oxidation of Li_2S to Li_2S_6 and the second oxidation peak at 0.25 V is due to the conversion of Li_2S_6 to sulfur. The two reduction peaks observed at -0.09 and -0.25 V are due to conversion of sulfur to Li_2S_6 and Li_2S_6 to Li_2S (Figure 4d).^[27,28] From these experiments, we can conclude that the G-NP is an efficient electrocatalyst. The batteries were fabricated using G-NP following the procedure used for other materials in this work. The cyclic voltammetry of the batteries fabricated using G-NP, sulfur, binder and conducting carbon showed typical redox peaks expected of sulfur. The decrease in peak current intensity (i_p) after five cycles is 5.8% (Supporting Information, Figure S11). This i_p decrease is the lowest among all the DLC-Gstudied in this work. The absorption solution studies and cyclic voltammetry studies of batteries confirm the suppression of polysulfide dissolution due to polyvalent electrostatic attraction between G-NP and polysulfides. The sharp peaks at 2.43 V in the cyclic voltammogram also indicates the electrocatalytic property of G-NP. The electrocatalytic activity is attributed to the presence of high percentage of pyridinic (38.9%) and graphitic nitrogen (32.4%). In the charge-discharge experiment, the specific capacity at the first cycle was 1345 mAh g^{-1} (0.2 h^{-1}). This specific capacity is 80% of theoretical maximum (Figure 5a). At the 100th cycle, the specific capacity decreased to 1084 mAh g^{-1} . The decrease is mere 20%. Unlike other DLC–G, the specific capacity of the first cycle remained above 1000 mAh g^{-1} at high C rates such as 2 h^{-1} (1218 mAh g^{-1}). Furthermore, the decrease in specific capacity as a function of hundred charge-discharge cycles varied as follows,13% (0.5 h^{-1}), 21% (1 h^{-1}), 20% (2 h^{-1}), 7% (5 h^{-1}). The lowest specific capacity of 815 mAh g^{-1} was found for batteries cycled at 5 h^{-1} . This impressive performance is due to polyvalent attraction between Ni ions on the layer of graphene with polysulfide. Please note that the discharge curves don't show any polarization due to electrocatalysis and suppressed dissolution of polysulfide. To further test the efficacy of batteries comprising G-NP, rate performance experiments were conducted. The specific capacity was 1279 mAh g^{-1} (0.1 h^{-1}) at the start of the experiment, which decreased to 324 mAh g^{-1} .

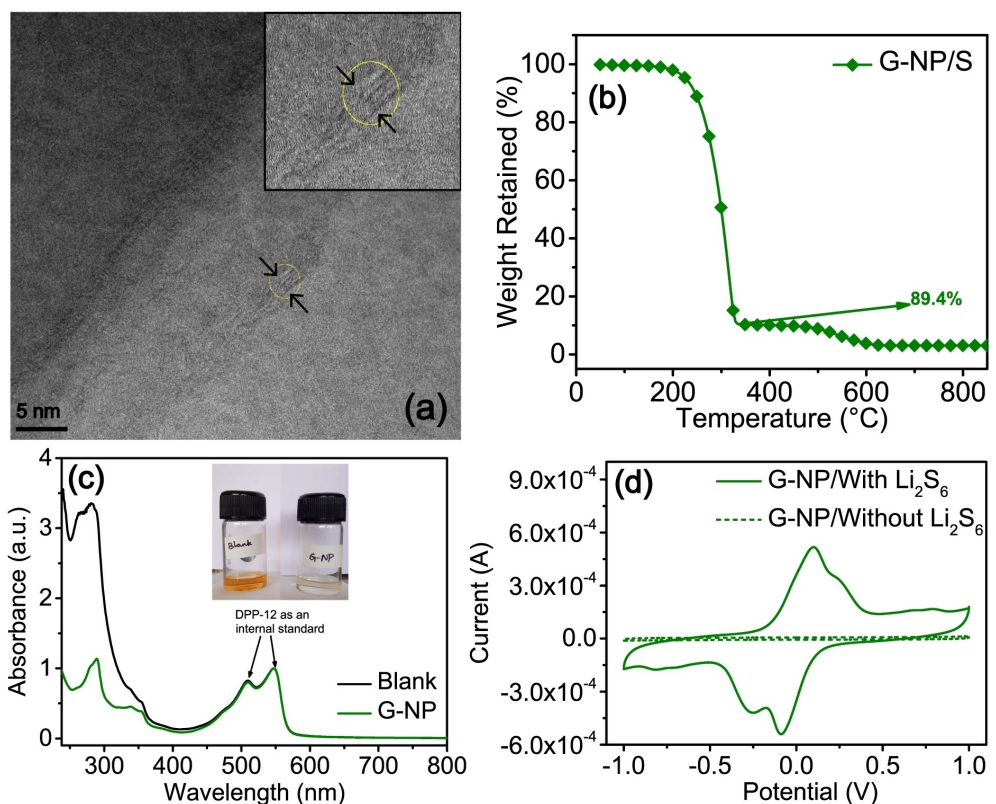


Figure 4. TEM image of G-NP showing few layer graphene (a). Thermogram of sulfur loaded G-NP (b). UV-vis absorption spectra of Li_2S_6 in presence and absence of G-NP. The insert shows colorless solution due to adherence of Li_2S_6 on G-NP. The yellow color solution doesn't comprise G-NP (c). Cyclic voltammogram of symmetric cells comprising G-NP with and without Li_2S_6 (d).

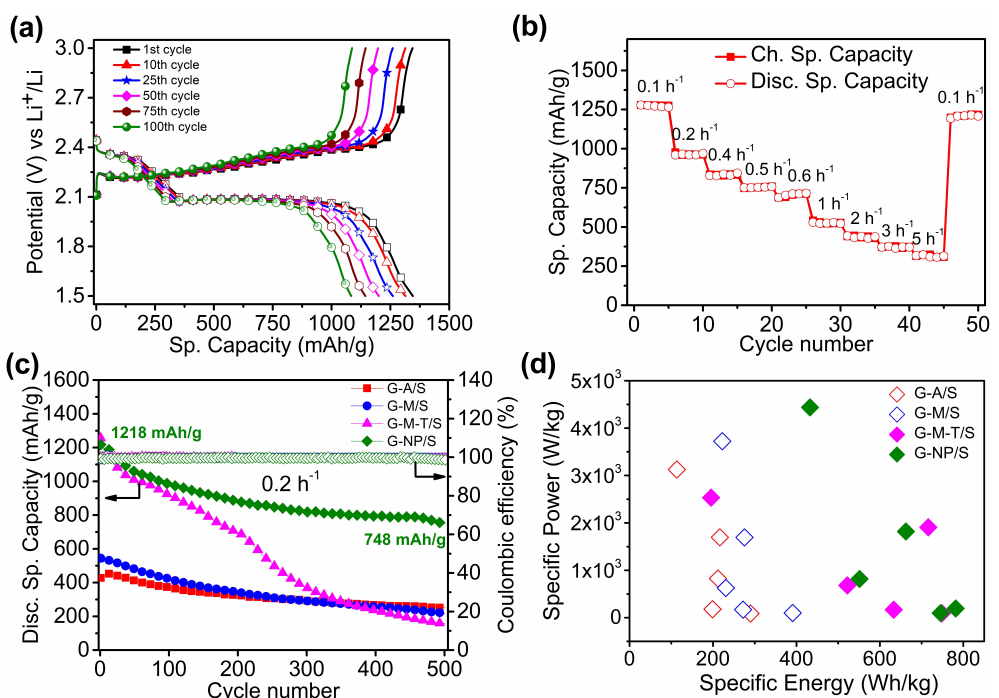


Figure 5. Charge-discharge profile at 0.2 h⁻¹ (a) and rate performance of Li-S cell comprising G-NP (b). Plot showing variation in specific capacity for 500 cycles 0.2 h⁻¹ (c). Ragone plot of Li-S batteries with various DLC-Gs (d).

(5 h⁻¹). Immediately after cycling at 5 h⁻¹, the experiment was conducted at 0.1 h⁻¹. In this experiment, the specific capacity bounced back to 1214 mAh g⁻¹ (Figure 5b). The loss of specific capacity is a mere 6% while going from 0.1 to 0.1 h⁻¹ through 0.2, 0.4, 0.5, 0.6, 1, 2, 3 and 5 h⁻¹. The data corroborates our hypothesis that the Ni ions on the layer of graphene withhold the polysulfide during the charge-discharge cycling experiments. To further study the cycling stability of G-NP based batteries, they were subjected to five hundred charge-discharge cycles. The G-NP based batteries' specific capacity decreased by 39% and the exact value of specific capacity was 748 mAh g⁻¹ (Figure 5c). Contrary to this, G-M-T based batteries exhibited initial specific capacity comparable to that of G-NP based batteries. However, at the end of five hundred charge-discharge cycles, the absolute specific capacity was 156 mAh g⁻¹, which is 4.7 times lower than that observed for G-NP based batteries. The decrease is a massive 88% for G-M-T based batteries. In the case of G-M and G-A based batteries, the initial specific capacity was low. Their specific capacity fading over 500 charge-discharge cycling is also comparable. G-M batteries show a slightly better performance than the G-A based batteries. The performance enhancement in case of G-M-T based batteries at the beginning of charge discharge experiment is impressive. But the fading in specific capacity as a function of cycle number is very high. Thus, the overall battery performance of G-M-T batteries is moderate. However, the overall performance of G-NP based batteries is very impressive. From the available data, we computed Ragone plot by calculating specific power and energy. The G-A and G-M based batteries showed very high specific power but exhibited poor specific energy. Contrary to this, the G-M-T and G-NP based batteries exhibited high specific energy. Specific energy equals the multiplication of cell voltage and amount of charge stored. The cell voltage is very close for all the batteries. However, the amount of charge stored is high for G-M-T and G-NP. Therefore, the batteries based on G-M-T and G-NP also showed high specific energy (Figure 5d). In addition, the batteries with G-NP exhibited high specific power (4437 W kg⁻¹) also. The specific energy is 782 Wh kg⁻¹ (Figure 5d).

3. Conclusions

In conclusion, we have developed an approach to prepare graphene with a layer comprising heteroatoms by employing a mechanical exfoliation process. The process utilizes exfoliators during the exfoliation of graphene from the pristine graphite. By judicious choice of exfoliator, DLC-G with nitrogen and DLC-G with nitrogen and sulfur are prepared. The battery with DLC-G comprising nitrogen and sulfur showed improved specific capacity compared to battery comprising DLC-G with nitrogen alone. However, the polysulfide dissolution is not suppressed. The DLC-G with Ni cations and nitrogen showed impressive specific capacity, power and energy density. This has been attributed to electrocatalysis facilitated by high percentage of pyridinic nitrogen. The suppression of sulfur dissolution is

attributed to electrostatic polyvalent attraction between Ni cations and polysulfide.

Experimental Section

Chemicals and materials

Graphite powder (Sigma-Aldrich, < 20 µm), Melamine (Alfa Aesar, 99%), Anthracene (Alfa Aesar, 99%), Ni-Phthalocyanine (Sigma-Aldrich, Dye content ca. 85%), 3-Thiopheneacetic acid (Sigma-Aldrich, 99%), Dimethylformamide (DMF, Merck, AR grade), Triton X-100 (Sigma-Aldrich, LR grade), Sodium thiosulfate (anhydrous, 99%), Hydrochloric acid (HCl, Merck, AR grade, 37%), Super P carbon (Imerys Graphite & Carbon Switzerland Ltd., Switzerland), polyvinylidluoride (PVDF, Kynar HSV900, Arkema Inc., USA), N-Methyl-2-pyrrolidone (NMP, Merck, AR grade), Celgard 2325 (Polypore, USA), Bis(trifluoromethane)sulfonimide lithium salt (LiTFSI, Sigma-Aldrich, 99.95%), Lithium nitrate (LiNO₃, Sigma-Aldrich, 99.99%), 1,3-dioxolane (DOL, Sigma-Aldrich, 99.8%), 1,2-dimethoxyethane (DME, Sigma-Aldrich, 99.5%) and Chloroform (Merck, AR grade) were purchased and used without further purification.

Exfoliation of graphite

The few-layer Graphene was prepared through a mechanical exfoliation process using the planetary mill (FRITSCH, PULVERISSETTE 6). The graphite powder was exfoliated using various exfoliating agents such as Melamine, Anthracene and Ni-Phthalocyanine (Scheme S1).

Samples 1–4

Graphite powder (1.5 g) and Melamine (7.5 g) were placed in an Agate ball mill grinder (250 mL) with six balls (1 cm diameter). The ball milling conditions are mentioned in Table S2 for respective samples. The as-prepared material was washed with a copious amount of Dimethylformamide (DMF) for an hour to remove the excess amount of melamine present in it and filtered and dried at 60 °C under vacuum for 16 h.

Samples 5–8

Graphite powder (1.5 g) and Anthracene (7.5 g) were chosen and followed the same procedure, and the milling conditions were mentioned in Table S2.

Samples 9–12

Graphite powder (1.5 g) and Ni-Phthalocyanine (7.5 g) were used and followed the same procedure and the milling conditions were mentioned in Table S2.

Synthesis of G-M, G-M-T, G-A and G-NP

G-M was obtained by carbonizing sample 4 at 600 °C under an Argon atmosphere for 4 h with the heat flow of 5 °C min⁻¹. For G-M-T, Sample 4 (9 g) was further ball milled with 3-Thiophene acetic acid (4.5 g) for 60 min with the speed of 200 rpm, washed with DMF, filtered and dried at 60 °C under vacuum for 16 h. Then carried out for carbonization at 600 °C under an Argon atmosphere for 4 h with the heat flow of 5 °C min⁻¹. G-A was obtained by carbonizing sample 8 at 600 °C under an Argon atmosphere for 4 h

with heat flow of $5^{\circ}\text{Cmin}^{-1}$. For G-NP, Sample 12 was carbonized at 600°C under an Argon atmosphere for 4 h with the heat flow of $5^{\circ}\text{Cmin}^{-1}$.

Synthesis of sulfur composite materials

The Sulfur particles were synthesized by the wet chemical process. In this method, 9 mL of Triton X-100 (1 wt%) was added into aqueous sodium thiosulfate (300 mL, 0.05 M) and the solution was heated at 70°C , followed by 10%HCl solution (30 mL) was slowly added into the above solution under vigorous magnetic stirring. The suspension of doped layer comprising graphene (DLC-G) (72 mg) in 100 mL of de-ionized water, was added drop-wise under magnetic stirring. After 15 min, the solution was cooled down to room temperature, filtered under vacuum with a copious amount of de-ionized water, dried at 60°C for 16 h.

Material characterizations

The TEM images were recorded with Tecnai G2 20 S-TWIN transmission electron microscope and HRTEM images were recorded with a Jeol 1200 EX transmission electron microscope. The carbon-coated copper grids (400 grids) were obtained from Ted Pella. E-SEM images were recorded using Quanta 200 and FESEM imaged were recorded with Nova Nano 450, both the instruments from the FEI company. The sample preparation for TEM and SEM were performed by preparing the 1 mg of sample dispersed in DMF and drop cast on the carbon-coated copper grid and silicon wafer are respectively. After the solvent evaporation, the substrates were kept at 40°C for 12 h and then performed the characterizations. The Raman spectroscopy measurements were performed with the help of a LabRam spectrometer (HJY, France) equipped with a laser wavelength of 632 nm. PANalytical instrument was operated using Cu K_{α} radiation ($\lambda = 1.542 \text{ \AA}$) at a scanning rate of $2^{\circ} \text{ min}^{-1}$ and a step size of 0.02° in 2θ with operating voltage 40 kV and operating current 30 mA to acquire the X-ray diffraction spectra. XPS measurements for the materials were done on Thermo Kalpha+ spectrometer using Al K_{α} radiation with an energy of 1486.6 eV. All the spectra were charge corrected with reference to C1s at 284.6 eV. The peak fittings were carried out using CasaXPS software. Thermogravimetric analyzes were carried out on SDTQ600 TG-DTA analyzer in a nitrogen environment with a ramp of $5^{\circ}\text{Cmin}^{-1}$.

Electrochemical measurements

The sulfur composite materials were used for battery application. The slurry for the cathode was prepared using the DLC-G, Super P carbon and PVDF are mixed with the mass ratio of 60:30:10, in N-methyl-2-pyrrolidone (NMP) solvent. The slurry was coated onto carbon-coated aluminium foil, allowed to dry at room temperature and dried at 60°C for 16 h. The above-prepared electrode was used as a working electrode, Li foil as counter and reference electrode and Celgard 2325 as separator (Thickness 25 μm). 1.0 M LiTFSI in 1,3-dioxolane and 1,2-dimethoxyethane (volume ratio 1:1) and 0.4 M LiNO₃ was used as an electrolyte. The 2032 type coin cells were fabricated in an Argon filled glovebox (MBRAUN, O₂<0.1 ppm, H₂O<0.1 ppm). The cyclic voltammetry was carried out using a multichannel Autolab MAC80038 instrument with the potential range of 1.5–3.0 V and the charge-discharge at the various current rate was carried out using the Neware battery testing system. All the electrochemical tests were carried out at 25°C . Graphically, the Specific energy (Wh kg^{-1}) was calculated from area under the discharge curve and Specific power (W kg^{-1}) was calculated by specific energy/time (h) of the discharge curve.

Symmetrical cell assembly and tests

A 0.2 M Li₂S₆ solution was prepared by dissolving elemental sulfur and Li₂S (5:1 molar ratio) in a mixture of DOL and DME (volume ratio of 1:1) under vigorous stirring at 50°C . The symmetrical cells were fabricated using identical DLC-Gs. The cells were assembled inside an Argon filled glovebox and CV tests were conducted for the symmetric cells with potential window of -1 to 1 V at 5 mVs^{-1} .

Acknowledgements

K.K. thanks Science and Engineering Research Board for financial support (EMR/2016/004732). S.K. thanks Department of Science and Technology for Inspire fellowship.

Conflict of Interest

The authors declare no conflict of interest.

Keywords: Electrocatalysis • graphene • mechanical exfoliation • polyvalent interaction • lithium-sulfur battery

- [1] P. g. Bruce, S. A. Freunberger, L. J. Hardwick, J.-M. Tarascon, *Nat. Mater.* **2012**, *11*, 19–29.
- [2] a) A. Manthiram, S.-H. Chung, C. Zu, *Adv. Mater.* **2015**, *27*, 1980–2006; b) A. Manthiram, Y. Fu, S.-H. Chung, C. Zu, Y.-S. Su, *Chem. Rev.* **2014**, *114*, 11751–11787; c) Y.-X. Yin, S. Xin, Y.-G. Guo, L.-J. Wan, *Angew. Chem. Int. Ed.* **2013**, *52*, 13186–13200; *Angew. Chem.* **2013**, *125*, 13426–13441; d) J. Kim, D.-J. Lee, H.-G. Jung, Y.-K. Sun, J. Hassoun, B. Scrosati, *Adv. Funct. Mater.* **2013**, *23*, 1076–1080; e) A. Rosenman, E. Markevich, G. Salitra, D. Aurbach, A. Garsuch, F. F. Chesneau, *Adv. Energy Mater.* **2015**, *5*, 1500212; f) F. Cerdas, P. Titscher, N. Bognar, R. Schmuck, M. Winter, A. Kwade, C. Herrmann, *Energies* **2018**, *11*, 150; g) Y. Zhang, P. Zhang, S. Zhang, Z. Wang, N. Li, S. R. P. Silva, G. Shao, *InfoMat.* **2021**, *3*, 790–803; h) C. Zhang, L. Cui, S. Abdolhosseinzadeh, J. Heier, *InfoMat.* **2020**, *2*, 613–638; i) Y.-X. Yao, X.-Q. Zhang, B.-Q. Li, C. Yan, P.-Y. Chen, J.-Q. Huang, Q. Zhang, *InfoMat.* **2020**, *2*, 379–388; j) Z. Wei, Y. Ren, J. Sokolowski, X. Zhu, G. Wu, *InfoMat.* **2020**, *2*, 483–508; k) Y. Dai, W. Zheng, X. Li, A. Liu, W. Zhang, X. Jiang, X. Wu, J. Tao, G. He, *ACS Appl. Mater. Interfaces* **2021**, *13*, 2521–2529; l) X. Li, Y. Zhang, S. Wang, Y. Liu, Y. Ding, G. He, N. Zhang, G. Yu, *Nano Lett.* **2020**, *20*, 701–708; m) Y. Liu, X. Li, Y. Liu, W. Kou, W. Shen, G. He, *Chem. Eng. J.* **2020**, *382*, 122858.
- [3] a) C. Liang, N. J. Dudney, J. Y. Howe, *Chem. Mater.* **2009**, *21*, 4724–4730; b) S. S. Zhang, *J. Power Sources* **2013**, *231*, 153–162.
- [4] a) J. Liang, Z.-H. Sun, F. Li, H.-M. Cheng, *Energy Storage Mater.* **2016**, *2*, 76–106; b) S. Jeong, D. Bresser, D. Buchholz, M. Winter, S. Passerini, *J. Power Sources* **2013**, *235*, 220–225; c) J. Schuster, G. He, B. Mandlmeier, T. Yim, K. T. Lee, T. Bein, L. F. Nazar, *Angew. Chem. Int. Ed.* **2012**, *51*, 3591–3595; *Angew. Chem.* **2012**, *124*, 3651–3655; d) X. Ji, K. T. Lee, L. F. Nazar, *Nat. Mater.* **2009**, *8*, 500–506.
- [5] a) A. Manthiram, Y. Fu, Y.-S. Su, *Acc. Chem. Res.* **2013**, *46*, 1125–1134; b) M. Li, J. E. Frerichs, M. Kolek, W. Sun, D. Zhou, C. J. Huang, B. J. Hwang, M. R. Hansen, M. Winter, P. Bieker, *Adv. Funct. Mater.* **2020**, *30*, 1910123; c) Y. V. Mikhaylik, J. R. Akridge, *J. Electrochem. Soc.* **2004**, *151*, A1969.
- [6] S.-H. Chung, A. Manthiram, *Adv. Mater.* **2014**, *26*, 7352–7357.
- [7] H. Yao, K. Yan, W. Li, G. Zheng, D. Kong, Z. W. Seh, V. K. Narasimhan, Z. Liang, Y. Cui, *Energy Environ. Sci.* **2014**, *7*, 3381–3390.
- [8] a) H. M. Kim, H.-H. Sun, I. Belharouak, A. Manthiram, Y.-K. Sun, *ACS Energy Lett.* **2016**, *1*, 136–141; b) B. Zhang, X. Qin, G. R. Li, X. P. Gao, *Energy Environ. Sci.* **2010**, *3*, 1531–1537; c) N. Jayaprakash, J. Shen, S. S. Moganty, A. Corona, L. A. Archer, *Angew. Chem. Int. Ed.* **2011**, *50*, 5904–5908; *Angew. Chem.* **2011**, *123*, 6026–6030.
- [9] a) X. Liang, C. Hart, Q. Pang, A. Garsuch, T. Weiss, L. F. Nazar, *Nat. Commun.* **2015**, *6*, 5682; b) Y. Tsao, Z. Chen, S. Rondeau-Gagné, Q.

- Zhang, H. Yao, S. Chen, G. Zhou, C. Zu, Y. Cui, Z. Bao, *ACS Energy Lett.* **2017**, *2*, 2454–2462; c) Y. Yang, G. Yu, J. J. Cha, H. Wu, M. Vosgueritchian, Y. Yao, Z. Bao, Y. Cui, *ACS Nano* **2011**, *5*, 9187–9193.
- [10] Z. Wu, W. Wang, Y. Wang, C. Chen, K. Li, G. Zhao, C. Sun, W. Chen, L. Ni, G. Diao, *Electrochim. Acta* **2017**, *224*, 527–533.
- [11] a) G. Zheng, Q. Zhang, J. J. Cha, Y. Yang, W. Li, Z. W. Seh, Y. Cui, *Nano Lett.* **2013**, *13*, 1265–1270; b) H. Wang, Y. Yang, Y. Liang, J. T. Robinson, Y. Li, A. Jackson, Y. Cui, H. Dai, *Nano Lett.* **2011**, *11*, 2644–2647.
- [12] a) C. Zu, A. Manthiram, *Adv. Energy Mater.* **2013**, *3*, 1008–1012; b) J. S. Lee, A. Manthiram, *J. Power Sources* **2017**, *343*, 54–59; c) H. Chen, C. Wang, Y. Dai, S. Qiu, J. Yang, W. Lu, L. Chen, *Nano Lett.* **2015**, *15*, 5443–5448; d) P. Shi, Y. Wang, X. Liang, Y. Sun, S. Cheng, C. Chen, H. Xiang, *ACS Sustainable Chem. Eng.* **2018**, *6*, 9661–9670; e) Y. Xie, Z. Meng, T. Cai, W.-Q. Han, *ACS Appl. Mater. Interfaces* **2015**, *7*, 25202–25210; f) D. Liu, C. Zhang, G. Zhou, W. Lv, G. Ling, L. Zhi, Q.-H. Yang, *Adv. Sci.* **2018**, *5*, 1700270.
- [13] a) A. Gomez-Martin, J. Martinez-Fernandez, M. Ruttert, M. Winter, T. Placke, J. Ramirez-Rico, *Carbon* **2020**, *164*, 261–271; b) P. Zhu, J. Song, D. Lv, D. Wang, C. Jaye, D. A. Fischer, T. Wu, Y. Chen, *J. Phys. Chem. C* **2014**, *118*, 7765–7771; c) F. Pei, T. An, J. Zang, X. Zhao, X. Fang, M. Zheng, Q. Dong, N. Zheng, *Adv. Energy Mater.* **2016**, *6*, 1502539.
- [14] V. León, M. Quintana, M. A. Herrero, J. L. g. Fierro, A. d l Hoz, M. Prato, E. Vázquez, *Chem. Commun.* **2011**, *47*, 10936–10938.
- [15] V. León, A. M. Rodriguez, P. Prieto, M. Prato, E. Vázquez, *ACS Nano* **2014**, *8*, 563–571.
- [16] a) C. Teng, D. Xie, J. Wang, Z. Yang, G. Ren, Y. Zhu, *Adv. Funct. Mater.* **2017**, *27*, 1700240; b) Y. Dong, S. Zhang, X. Du, S. Hong, S. Zhao, Y. Chen, X. Chen, H. Song, *Adv. Funct. Mater.* **2019**, *29*, 1901127.
- [17] Q. Pang, L. F. Nazar, *ACS Nano* **2016**, *10*, 4111–4118.
- [18] a) G. Zhou, E. Paek, G. S. Hwang, A. Manthiram, *Nat. Commun.* **2015**, *6*, 7760; b) J. Balach, H. K. Singh, S. Gomoll, T. Jaumann, M. Klose, S. Oswald, M. Richter, J. Eckert, L. Giebelner, *ACS Appl. Mater. Interfaces* **2016**, *8*, 14586–14595; c) X. Zhou, Q. C. Liao, T. Bai, J. Yang, *J. Mater. Sci.* **2017**, *52*, 7719–7732.
- [19] L. Kong, B.-Q. Li, H.-J. Peng, R. Zhang, J. Xie, J.-Q. Huang, Q. Zhang, *Adv. Energy Mater.* **2018**, *8*, 1800849.
- [20] a) S. Niu, W. Lv, C. Zhang, F. Li, L. Tang, Y. He, B. Li, Q.-H. Yang, F. Kang, *J. Mater. Chem. A* **2015**, *3*, 20218–20224; b) M. Zhang, C. Yu, J. Yang, C. Zhao, Z. Ling, J. Qiu, *J. Mater. Chem. A* **2017**, *5*, 10380–10386; c) J.-L. Shi, C. Tang, J.-Q. Huang, W. Zhu, Q. Zhang, *J. Energy Chem.* **2018**, *27*, 167–175.
- [21] D. M. Koshy, S. Chen, D. U. Lee, M. B. Stevens, A. M. Abdellah, S. M. Dull, G. Chen, D. Nordlund, A. Gallo, C. Hahn, D. C. Higgins, Z. Bao, T. F. Jaramillo, *Angew. Chem. Int. Ed.* **2020**, *59*, 4043–4050; *Angew. Chem.* **2020**, *132*, 4072–4079.
- [22] A. Eckmann, A. Felten, A. Mishchenko, L. Britnell, R. Krupke, K. S. Novoselov, C. Casiraghi, *Nano Lett.* **2012**, *12*, 3925–3930.
- [23] a) G. George, S. B. Sisupal, T. Tomy, B. A. Pottammal, A. Kumaran, V. Suvekbalra, R. Gopimohan, S. Sivaram, L. Ragupathy, *Carbon* **2017**, *119*, 527–534; b) G. George, S. B. Sisupal, T. Tomy, A. Kumaran, P. Vadivelu, V. Suvekbalra, S. Sivaram, L. Ragupathy, *Sci. Rep.* **2018**, *8*, 11228.
- [24] R. Blume, D. Rosenthal, J.-P. Tessonner, H. Li, A. Knop-Gericke, R. Schlögl, *ChemCatChem* **2015**, *7*, 2871–2881.
- [25] a) W. Li, J. Qian, T. Zhao, Y. Ye, Y. Xing, Y. Huang, L. Wei, N. Zhang, N. Chen, L. Li, F. Wu, R. Chen, *Adv. Sci.* **2019**, *6*, 1802362; b) J. He, Y. Chen, A. Manthiram, *iScience* **2018**, *4*, 36–43.
- [26] D. Tian, X. Song, M. Wang, X. Wu, Y. Qiu, B. Guan, X. Xu, L. Fan, N. Zhang, K. Sun, *Adv. Energy Mater.* **2019**, *9*, 1901940.
- [27] L. Zhang, D. Liu, Z. Muhammad, F. Wan, W. Xie, Y. Wang, L. Song, Z. Niu, J. Chen, *Adv. Mater.* **2019**, *31*, 1903955.
- [28] a) R. Wang, C. Luo, T. Wang, G. Zhou, Y. Deng, Y. He, Q. Zhang, F. Kang, W. Lv, Q.-H. Yang, *Adv. Mater.* **2020**, *32*, 2000315; b) Z. Liang, D. Yang, P. Tang, C. Zhang, J. Jacas Biendicho, Y. Zhang, J. Llorca, X. Wang, J. Li, M. Heggen, J. David, R. E. Dunin-Borkowski, Y. Zhou, J. R. Morante, A. Cabot, J. Arbiol, *Adv. Energy Mater.* **2021**, *11*, 2003507; c) J. He, A. Bhargav, A. Manthiram, *ACS Nano* **2021**, *15*, 8583–8591.

Manuscript received: August 28, 2021

Revised manuscript received: October 18, 2021

Accepted manuscript online: October 25, 2021

Version of record online: November 15, 2021